J Mater Sci (2007) 42:6779–6786
DOI 10.1007/s10853-006-1464-y

A study on the synthesis and characterisation of nanocrystalline transition metal oxynitrides

Yuhong Wang · Edward Lesterb · Duncan H. Gregory

Received: 16 May 2006 / Accepted: 15 December 2006 / Published online: 26 April 2007

Abstract A different processing route to bimetallic oxynitrides has been developed using oxide precursors generated from coprecipitation of ethanolic solutions of the relevant metal chlorides. The nitridation of the mixed-metal precursors yields nanocrystalline oxynitrides. Representative group 5–group 6 transition metal oxynitrides, $M_{1-x}M'_x(O,N)$ (M = Nb, Ta; M′ = Mo, W) have been prepared and characterised by powder X-ray diffraction (PXD), scanning electron microscopy with energy dispersive analysis by X-rays (SEM/EDAX), transmission electron microscopy (TEM) with selected area electron diffraction (SAED), BET surface area measurements and SQUID magnetometry. The mixed-metal oxynitrides form rock salt structures (a ~4.3 Å) with disordered distributions of both cations and anions. The purity, particle size and surface area of materials are significantly dependent on nitridation temperature.

Y. Wang (✉)
Department of Chemical Engineering, Shanghai Institute of Technology, 200235 Shanghai, P.R. China
e-mail: yuhong_wang502@hotmail.com

E. Lesterb
School of Chemical, Environmental and Mining Engineering, University of Nottingham, Nottingham NG7 2RD, UK

D. H. Gregory
School of Chemistry, University of Nottingham, Nottingham NG7 2RD, UK

Introduction

Recently, transition metal nitrides and oxynitrides have attracted significant attention, not least because they exhibit technologically useful properties and consequently have found utility as ceramics, abrasives, pigments, electronic and magnetic materials, superconductors and catalysts [1–5]. Despite the potential technological importance of such materials, only a small number of nitrides and related mixed-anion compounds are known relative to oxides, for example [6–8]. Until recently, the synthetic challenges in preparing these compounds has restricted the focus of studies to binary (monometallic) nitrides. Emerging and maturing synthetic methodologies are now addressing this imbalance and permitting the in-depth investigations of more complex systems for the first time.

One area to benefit from this synthetic evolution is catalysis where it has been recognised for several decades that transition metal nitrides can rival the catalytic properties of the noble metals in hydrotreating processes [9]. The electronic structures of the heavier group 5 and 6 nitrides, of long academic interest in solid state chemistry and condensed matter physics [2], are remarkably similar to those of the existing commercial catalysts. The catalytic activity and selectivity in processes such as hydrodenitrogenation (HDN), hydrodesulphurisation (HDS) and the Fischer-Tropsch reaction is extremely sensitive to composition [10]. Research in recent years has concentrated increasingly on multimetallic and mixed anion systems to compositionally (and structurally) tune these properties [11–14]. Previous preparation methods based on powder metallurgy (and/or requiring high temperatures and pressures) are not conducive to catalytic applications and synthesis techniques towards high purity, high surface area solids need to be developed for this purpose.

The use of oxide or other inorganic precursors in nitridation reactions has been generally successful in the synthesis of binary and higher nitrides and mixed anion compounds under relatively mild conditions [7, 8, 15]. The structure, composition and nature of the precursor has played an increasingly important role both in governing the microstructure of the nitrided materials and crucially also in determining the *identity* itself of the resulting material. Over the last few years, particularly with the advent of the sol-gel process, there has been considerable interest in extending the solution chemistry approaches exploited in oxide chemistry to nitrides. The interest has been primarily due to the excellent molecular mixing that is possible in solution. As a result, precursors can be generated that have clusters or molecular structural units representing the ultimate desired material.

A number of recent studies have illustrated how ''soft chemistry'' and temperature programmed reaction approaches can be used to prepare nanoparticular bimetallic oxynitrides with high surface areas, high catalytic activity and/or promising mechanical properties [12, 13, 16–19]. Equally, similar techniques yield ternary nitrides and oxynitrides exhibiting metallic behaviour and/or cooperative magnetism, which could be of significant interest and then nano-regime [20–23]. In this work we report the synthesis, under relatively mild conditions, of bimetallic group 5 and 6 oxynitride nanoparticles from oxide precursors produce via coprecipitation methods. Optimised reaction conditions have allowed us to systematically characterise the composition, structure and morphology of the resulting some surface area oxynitrides and investigate the Ta–W–N–O system for the first time. The magnetic properties of the nanocrystalline materials were also investigated.

Experimental

Precursor synthesis

All inorganic metal chlorides were used as received: $TaCl_5$ (Aldrich, 99.99%), $MoCl_5$ (Aldrich, 98%), WCl_6 (Aldrich, 99.9+%) and $NbCl_5$ (Aldrich, 99.9+%).

The oxide precursors were prepared via a coprecipitation route. Initial Ta, Mo, W and Nb containing solutions were prepared by dissolving the respective chloride salts in ethanol. These were combined to obtain Ta–Mo, Ta–W and Nb–Mo with total cationic concentrations of 0.006 M, and nominal molar compositions Ta:Mo (Ta:W, Nb:Mo) = 1:1. The mixed solutions were stirred and heated at 333 K until the ethanol solvent had completely evaporated followed by further drying at 383 K for 2 h. In this way, dried solid materials were obtained as amorphous (by PXD) loose powders. The oxide precursors were obtained by heating the amorphous solid materials at 923 K for 12 h in air.

Oxynitride synthesis

Oxynitrides were synthesised by nitridation of the freshly prepared oxide precursors. A sample of the selected precursor (0.5 g) was placed into an alumina boat, which was then inserted into an alumina tube furnace for reaction under flowing ammonia gas. Prior to initiating the thermal treatment, the tube furnace was purged for 10 min with flowing argon gas and for an additional 5 min with gaseous ammonia.

Initially, several experiments with varying reaction parameters were performed in order to determine the appropriate conditions for the preparation of pure samples. The precursor powder was heated under flowing ammonia (100 cm^3 min^{-1}) at 5 $Kmin^{-1}$ to a final temperature, held at the reaction temperature for 2 h and finally allowed to furnace cool. After cooling, the product was always passivated with flowing argon gas for 10 min.

Bulk characterisation

PXD patterns were obtained from Philips X'Pert and Bruker D8 Advance (θ–2θ) diffractometers using CuK_α and $CuK_{\alpha 1}$ radiation, respectively. Routine patterns for phase identification were collected with a scanning step of 0.02°2θ over the angular range 5–80°2θ with typical collection times of 0.6 s $step^{-1}$. Phase purity was evaluated by reference to the ICDD Powder Diffraction File (PDF). Cell parameters were indexed from short scan (ca. 1 h) data over a similar 2θ range using DICVOL91 [24] and refined by least squares fitting of PXD data. Subsequent analysis of the diffraction patterns was made with POWDERCELL 2.3 [25] comparing experimental patterns to those calculated using models generated from experimental and literature data. Longer PXD scans were taken for this purpose, typically between 10 and 120°2θ with step size 0.02°2θ over ca. 12 h.

Microstructural characterisation and elemental analysis

The morphology of both the oxide precursors and the nitrided materials was examined using a Philips XL30 ESEM-FEG scanning electron microscope (SEM) equipped with an EDAX CDU LEAP detector operating at an accelerating voltage of 20 kV. Metal ratios in the solids were determined by energy dispersive X-ray analysis (EDAX) with quantification performed using virtual standards and associated DX4i software. The operating voltage was 20 kV, and the energy range for analysis 0–20 keV. The microstructures of the nitrided materials

were also investigated using a JEOL 2000FXII transmission electron microscope (TEM) with accelerating voltages up to 200 kV.

Surface area measurements

Surface areas were determined using gas adsorption techniques. Data were measured using nitrogen as the adsorptive at 77 K by conventional volumetric techniques using two instruments; a Micromeritics ASAP 2010 and a Coulter SA3100 sorptometer. Ca. 250 mg samples were used for each experiment and each sample was degassed for over 10 h at 393 K to remove moisture and other volatile impurities. The adsorption of nitrogen was measured over partial pressure (P/P_0) ranges of 0.05–0.2 (SA3100) or 0.01–1.0 (ASAP 2010). The BET method was used to calculate the surface areas of powders in $m^2\ g^{-1}$.

Magnetic measurements

The temperature dependence of the magnetic susceptibility was investigated for crystalline samples of each compound using a Quantum Design MPMS-XL 5T Superconducting Quantum Interference Device (SQUID) magnetometer. All samples (ca. 100–250 mg, accurately weighed) were loaded into gelatine capsules in a nitrogen-filled, dry glovebox. Data were collected as RSO (Reciprocating Sample Option) scans between 5 K and 300 K at an applied field of 1,000 Oe in increasing temperature increments (measurements were taken in 1 K intervals between 5 and 30 K, 2 K intervals between 30 K and 100 K, 3 K intervals between 100K and 200 K and 5 K intervals from 200 K to 300 K). Sufficient pauses were built in to allow for temperature equilibration at each data point. Data were corrected for core diamagnetism and the diamagnetic contribution of the sample containers.

Results and discussion

Oxide precursors

The oxide precursors were obtained by heating the amorphous solid materials prepared using coprecipitation methods at 923 K for 12 h. The heating regime yielded pale yellow (Mo–Ta, Ta–W) and grey-green powders (Nb–Mo) that were stable to air and moisture. The Mo–Ta and Ta–W precursors were characterised by powder X-ray diffraction and identified through the PDF database (ICDD) as $Mo_2Ta_2O_{11}$ (card No. 38–1368) and $Ta_{16}W_{18}O_{94}$ (card No. 29–1323) respectively. The former also contained small amounts of MoO_3 and Ta_2O_5. The vast majority of peaks in the Nb–Mo–O sample could be matched to ''$3MoO_2 \cdot Nb_2O_5$'' (card No. 18–840) with weaker intensity peaks attributable to Nb_2O_5. The ternary compound $Mo_3Nb_2O_{11}$ has been previously observed as a predominant phase at this reaction temperature in the Mo–V–Nb and Mo–V–Te–Nb oxide catalyst systems [26, 27]. A Nb–Mo oxide yielding an almost identical PXD pattern has been reported as the fully oxidised $Mo_3Nb_2O_{14}$ [28]. Our pattern matches well to those observed in these previous studies. Under our experimental conditions (and given the identity of the fully oxidised Mo–Ta and Ta–W oxides obtained under identical conditions) it seems more likely that $Nb_2Mo_3O_{14}$ is the correct stoichiometry of the 2:3 Nb:Mo oxide. No reports of a 1:1 compound in the ternary Nb–Mo–O system exist to our knowledge in the literature. PXD patterns of the oxide precursors are shown in Fig. 1a–c. The morphology of the oxide precursors was examined using SEM and typical micrographs are shown in Fig. 2. SEM images show that $Mo_2Ta_2O_{11}$ samples are composed of porous agglomerates (typically 50–200 μm across) and smaller rods (typically 5–10 μm in length). $Ta_{16}W_{18}O_{94}$ samples were composed of less porous blocks up to 50 μm across whereas $Nb_2Mo_3O_{14}$ samples comprised dense agglomerations of rods up to 5 μm in length and typically up to 1 μm across. The molar ratios of the metals from EDAX were determined as 1:1, 1:1.1 and 1:1.4 for Mo:Ta, Ta:W and Nb:Mo respectively and are in good agreement with the stoichiometry of the ternary precursors proposed on the basis of PXD results.

Synthesis and characterisation of nitrided materials

Reports in the literature demonstrate substantial evidence for the formation of different binary and particularly higher

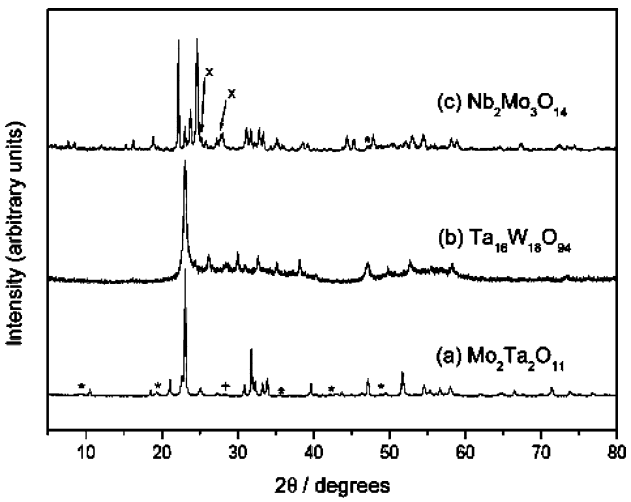

Fig. 1 PXD patterns of oxide precursors: (**a**) $Mo_2Ta_2O_{11}$, (**b**) $Ta_{16}W_{18}O_{94}$ and (**c**) $Nb_2Mo_3O_{14}$. Impurity phases are denoted as: MoO_3 (*), Ta_2O_5 (+) and Nb_2O_5 (×)

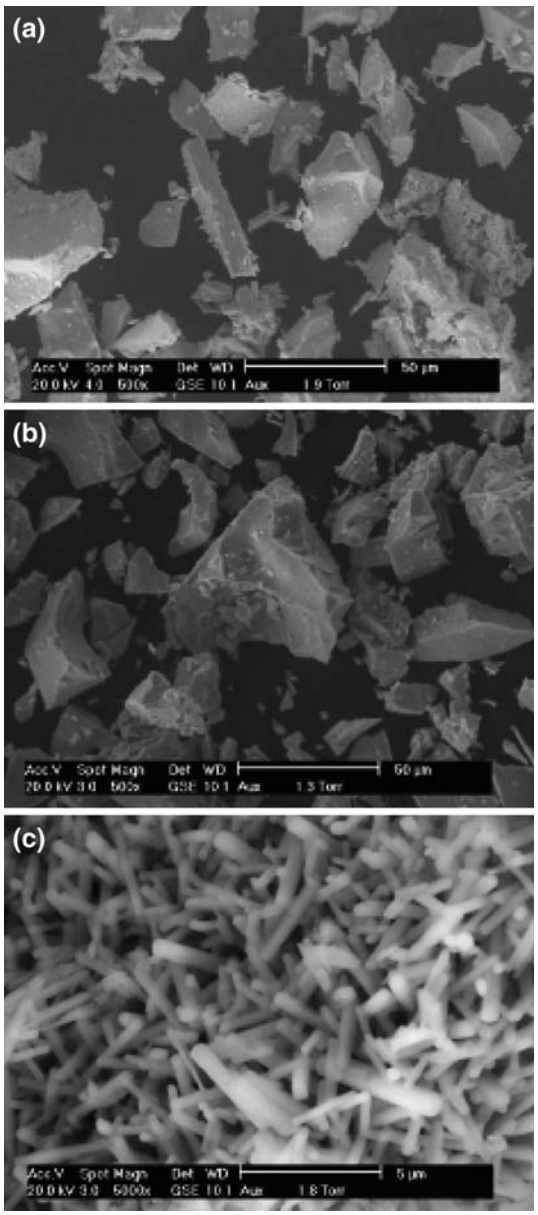

Fig. 2 SEM micrographs of oxide precursors: (**a**) $Mo_2Ta_2O_{11}$, (**b**) $Ta_{16}W_{18}O_{94}$ and (**c**) $Nb_2Mo_3O_{14}$

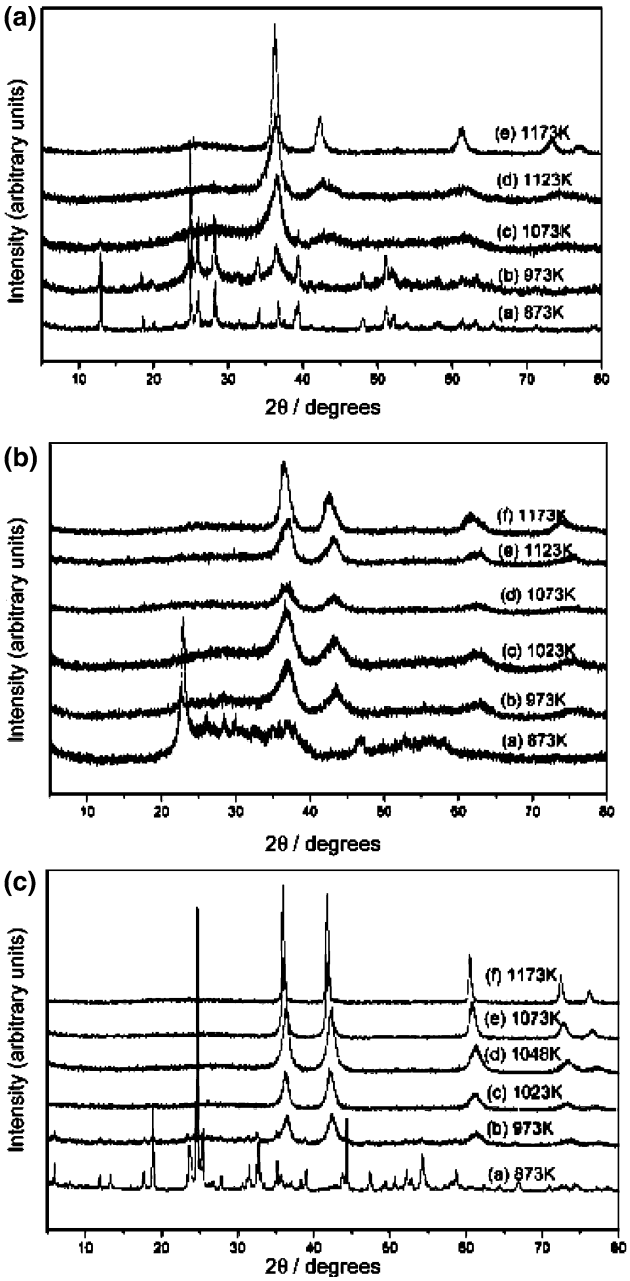

Fig. 3 PXD patterns of nitrided materials from oxide precursors with increasing reaction temperature, (**a**) Mo–Ta, (**b**) Ta–W and (**c**) Nb–Mo

nitrides and oxynitrides depending on both the experimental parameters and the nature of the metal precursor itself in nitridation reactions [9]. Thus, our first goal was to investigate the optimal conditions for obtaining single-phase ternary nitrides from our precursors. We performed preliminary nitridation reactions from the oxide precursors using fixed, short reaction times of 2 h, eliminating time as a variable and following the precedent of Himri et al. [18] in the synthesis of $V_{1-z}Mo_z(O_xN_y)$. Temperatures ranging from 873 K to 1,173 K were employed utilising temperature programmed ramp rates and slow cooling rates in our preparative procedure. Figure 3 shows the PXD patterns of the black nitrided materials after treatment at the indicated temperatures. Single-phase products were obtained between 1,123 K and 1,173 K in the Ta–Mo system whereas single-phase Ta–W and Nb–Mo compounds are obtained at temperatures between 1,023 K and 1,173 K. From the above experiments, we selected nitridation temperatures of 1,123, 1,023 and 1,048 K as the minimum required to prepare Ta–Mo, Ta–W and Nb–Mo compounds respectively as pure phases of small particle size (judged

qualitatively from peak widths in PXD patterns at this point).

The identity of the nitrided materials was first investigated by comparisons of powder patterns with those in the PDF database. On this basis while the nitrided Mo–Ta and Mo–Nb compounds were tentatively identified as $Mo_{1.5}Ta_{1.5}N_2$ (Card No. 75–2338) and $MoNbN_{0.9}$ (Card No. 86–1566) respectively, no match was found to the Ta–W compound. Visual comparison of the patterns suggested all three compounds were likely to be isostructural. Closer inspection of our experimental patterns (particularly those of higher crystallinity prepared at higher temperature) revealed weaker reflections from the previously reported Mo–Ta and Mo–Nb tetragonal phases above were not present in our data. This was confirmed further by superimposing calculated patterns generated from structural data using POWDERCELL 2.3 [25]. In fact, our patterns bore a great resemblance to those observed by Oyama et al. [13] for bimetallic oxynitrides previously designated ''$MI_wMII_xO_yN_z$''. Furthermore, the patterns also closely resemble those of rock-salt structured binary transition metal nitrides, MN (M = Ti, V, Cr, etc) [29]. The powder patterns were successfully indexed to the relevant face centred cubic unit cell with the lattice parameters described in Table 1. These cubic lattice parameters of ca. 4.3 Å are also in close agreement with nitrided materials previously identified as bimetallic nitrides such as $WNb_{12}N_x$ [14]. Metal ratios were obtained from EDAX point scan measurements of the nitrided materials and these are in good agreement with those of the precursors as expected (Table 1). Although no reliable quantitative EDAX data could be obtained for anion ratios, all point and area scans showed both N and O present in all samples. The approximate ratios of N:O were reasonably consistent over multiple scans at 3:2, 2:1 and 1:1 for Mo–Ta, Ta–W and Nb–Mo samples respectively. Elemental mapping confirmed even distributions of metals and anions across particles. Hence we ascribe the nitrided materials to be $M_{1-x}M'_x(O,N)$ bimetallic oxynitrides.

Using the above observations as a basis, the powder patterns of the most crystalline (highest temperature) materials were fit to generated patterns from POWDERCELL 2.3 using structural models in space group *Fm3m* with metals disordered on the *4b* site and O and N disordered on the *4a* site. The N:O ratio was set at the approximate values from EDAX and while small changes in ratio of these species inevitably has negligible effect on PXD patterns, it should be noted that the variations in N:O stoichiometry from EDAX scans could emanate in part from surface-absorbed oxygen. Although we saw no direct evidence of reaction of any oxynitride samples, this has been previously suggested to be the major source of oxygen content variation in bimetallic and trimetallic oxynitride compounds (as opposed to substantial changes in interstitial site population by oxygen) [18]. Powder neutron diffraction experiments should reveal more definitively the metal and nonmetal distributions in these materials. The experimental PXD patterns closely matched those calculated from the disordered rock-salt models. The observed and calculated patterns for $Nb_{1-x}Mo_x(O,N)$ ($x \approx 0.6$) are shown in Fig. 4.

Crystallite size and surface area for the oxynitrides are also shown in Table 1. Average crystallite sizes (D_c) for samples prepared at optimum temperature were calculated from the peak width of the (220) reflection in each pattern by application of the Scherrer equation. Instrumental peak width was taken from a silicon standard sample (FWHM 0.01°). Molybdenum containing oxynitrides yield very similarly sized crystallites < 10 nm across, yet despite the lower preparation temperature, $Ta_{1-x}W_x(O,N)$ crystallites are significantly larger. All three materials show high surface areas from BET measurements as would be expected for nanocrystallites. Particle size (D_p) was calculated from surface area values taking the density in each oxynitride as that derived from the PXD models with $\rho[Mo_{1-x}Ta_x(O,N)] = 12.98$ g cm^{-3}, $\rho[Ta_{1-x}W_x(O,N)] = 16.20$ g cm^{-3} and $\rho[Nb_{1-x}Mo_x(O,N)] = 8.98$ g cm^{-3}. The calculated D_p values are generally in good agreement with D_c values, although for Nb–Mo D_c is reduced by a factor of ~2.5 suggesting perhaps strain effects may also contribute to the PXD peak broadening.

Microstructural characterisation of oxynitrides

Figure 5 shows representative SEM micrographs at varying magnification of the three bimetallic oxynitride materials. At first sight the oxynitrides appear as porous blocks that at higher magnification are revealed to be agglomerates

Table 1 Compositional, structural and microstructural parameters for MM′(O,N) oxynitrides

Compound	Optimum reaction T/K	M:M′	α/Å	D_c/nm[a]	S_g/m^2 g^{-1}	D_p/nm[b]
$Mo_{1-x}Ta_x(O,N)$	1,123	1:1	4.276(1)	6.2	65.4	7.1
$Ta_{1-x}W_x(O,N)$	1,023	1:1.1	4.264(5)	25.2	22.4	16.5
$Nb_{1-x}Mo_x(O,N)$	1,048	1:1.5	4.326(1)	7.8	35.6	18.8

[a] $D_c = 0.9\lambda/(\beta \cos\theta)$;
[b] $D_p = 6/(\rho S_g)$

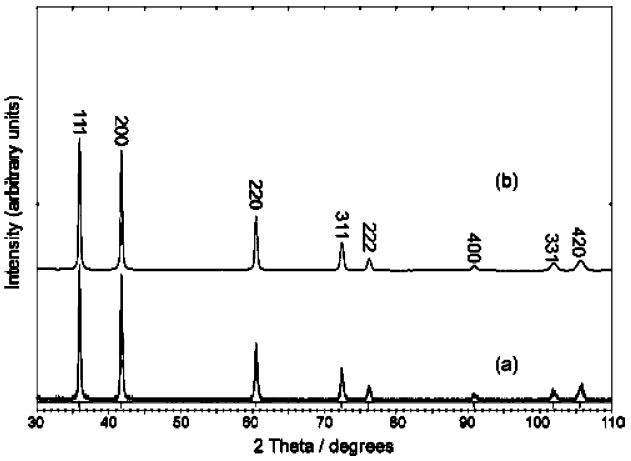

Fig. 4 Observed (**a**) and calculated (**b**) profiles for $Nb_{0.4}Mo_{0.6}N_{0.5}O_{0.5}$

of nanoscaled discs (Mo–Ta) spheres (Ta–W) or rods (Mo–Nb). There do not appear to be significant changes in crystallite morphology following nitridation—particularly for Mo-containing materials. For example, in the case of $Mo_{1-x}Ta_x(O,N)$ (Fig. 5a cf Fig. 2a), it can be seen that the porous appearance of the irregular blocks in the precursor are retained during the nitridation process Similarly, $Mo_{1-x}Nb_x(O,N)$ (Fig. 5c cf Fig. 2c) bears a close resemblance to the precursor; the oxide is comprised of short needles or rods whereas the oxynitride consists of a tangled mass of smaller rods with a slightly reduced aspect ratio following nitridation. The transformation from oxide to oxynitride for the Mo-containing materials is therefore ostensibly pseudomorphic as observed for the nitridation of MoO_3 to Mo_2N and V_2O_5 to VN [30, 31].

The crystallite sizes obtained from SEM are generally in broad agreement with those calculated from PXD (and inferred from BET measurements) within the range of the instrument. It is apparent from the micrographs at high magnification (e.g. up to 200 nm scale) that the materials are composed of groups of individual particles of the order of tens of nm. There is no obvious correlation of particle size with optimum reaction temperature *between* oxynitrides; indeed the smallest crystallites are obtained from the materials produced at the highest optimum temperature (Mo–Ta). As one would expect, SEM micrographs showed that the crystallite size increased with reaction temperature within each system.

A more accurate measure of individual crystallite size was obtained from TEM investigations. A representative micrograph is shown in Fig. 6a. Once dispersed on the

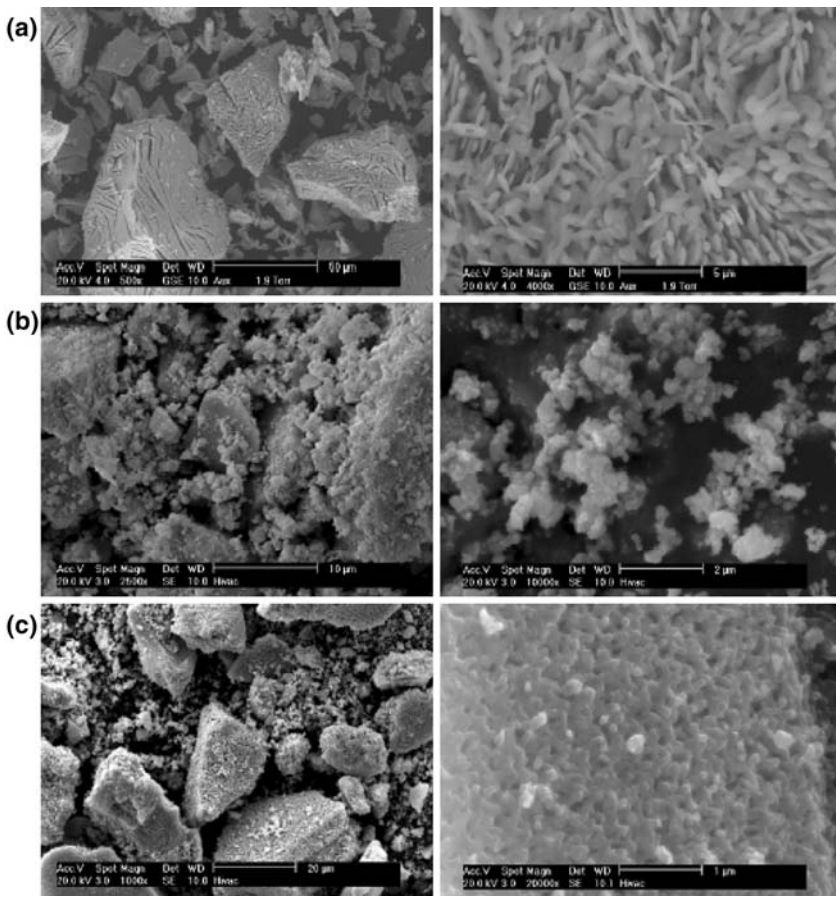

Fig. 5 SEM micrographs of nitrided materials at optimum reaction temperatures: (**a**) $Mo_{1-x}Ta_x(N,O)$, (**b**) $Ta_{1-x}W_x(N,O)$ and (**c**) $Nb_{1-x}Mo_x(N,O)$

TEM grid, samples were shown to be comprised of clusters of individual nanocrystals typically between 5 and 30 nm in dimension. This is in good agreement with PXD and BET calculations. Selected area electron diffraction (SAED) patterns were collected from nanocrystallites for each of the oxynitrides. The vast majority of these produced clear spot patterns representative of well-ordered, crystalline materials. Patterns were indexed to yield lattice parameters in good agreement with those derived from PXD measurements. For example, Fig. 6b shows the pattern taken for $Ta_{1-x}Mo_x(O,N)$ along the <111> zone axis. The pattern was indexed to a cube with $a \approx 4.3$ Å consistent with PXD results.

Magnetic measurements

Plots of the magnetic mass susceptibility as a function of temperature for samples of the three oxynitrides are shown in Fig. 7. The susceptibility profiles for the oxynitrides are very similar in form and magnitude. The low values of the magnetic susceptibility suggest Pauli paramagnetic behaviour typical of delocalised electron systems and indeed the susceptibility is essentially temperature independent between 100 K and 300 K. Below this temperature there is evidence of a Curie-like component suggesting some degree of electron localisation or, perhaps more likely, presence of paramagnetic impurity below detection limits of PXD and other analysis. The additional broad feature at ca. 50 K for Ta–W and Nb–Mo samples is ascribed to condensed oxygen. Good fits to the susceptibility for all three oxynitrides are obtained by modelling the behaviour as a mixture of Curie-like and temperature independent contributions, $\chi_g = \chi_0 + C_g/T$. The region corresponding to condensed oxygen was excluded from these fits. Attempts to fit Curie–Weiss contributions ($\chi_g = \chi_0 + C_g/[T + \theta]$) were unsuccessful, whereas errors in all parameters decreased and the fit improved markedly when θ was set at 0. This zero value is consistent with the absence of observed magnetic transitions in data for all three materials. The C_g values obtained for the $Mo_{1-x}Ta_x(O,N)$, $Ta_{1-x}W_x(O,N)$ and $Mo_{1-x}Nb_x(O,N)$ samples are $2.68(1) \times 10^{-5}$ emu g^{-1}, $6.83(5) \times 10^{-6}$ emu g^{-1} and $2.11(1) \times 10^{-5}$ emu g^{-1} respectively. The χ_0 values were calculated as $7.51(6) \times 10^{-7}$ emu g^{-1}, $1.28(2) \times 10^{-7}$ emu g^{-1} and $4.71(5) \times 10^{-7}$ emu g^{-1} respectively. These susceptibility profiles, low C_g values and positive χ_0 values are typical of those seen in Pauli paramagnetic, metallic, transition metal nitrides and oxynitrides. Co_3Mo_3N, for example, displays very similar susceptibility behaviour with temperature [32]. Interestingly, also, the rock-salt structured monometallic oxynitride, V(O,N) is weakly paramagnetic with a susceptibility behaviour that can be fit to Pauli and Curie magnetic contributions [22]. It was postulated that 10% of the V atoms in V(O,N) possess localised moments in this compound, although equally, as here, the Curie tail could be ascribed to low-level paramagnetic impurities. Such observations are not uncommon in ternary tantalum nitrides [33].

Conclusions

In summary, coprecipitation techniques have been used to prepare nanocrystalline bimetallic transition metal oxynitrides. These have allowed systematic characterisation of structure, morphology and properties and the first investigations of the Ta–W–N–O system. The resulting oxynitrides form rock salt structures with disordered cations and anions. The synthesis method yields nanosized particles with some surface areas and therefore potential as catalysts

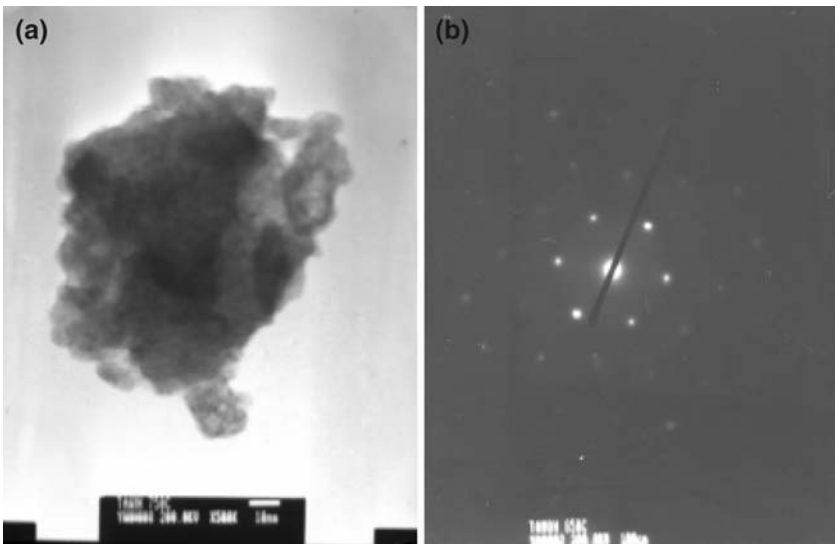

Fig. 6 (**a**) TEM micrograph of $Ta_{1-x}W_x(N,O)$ and (**b**) SAED pattern for $Ta_{1-x}Mo_x(N,O)$

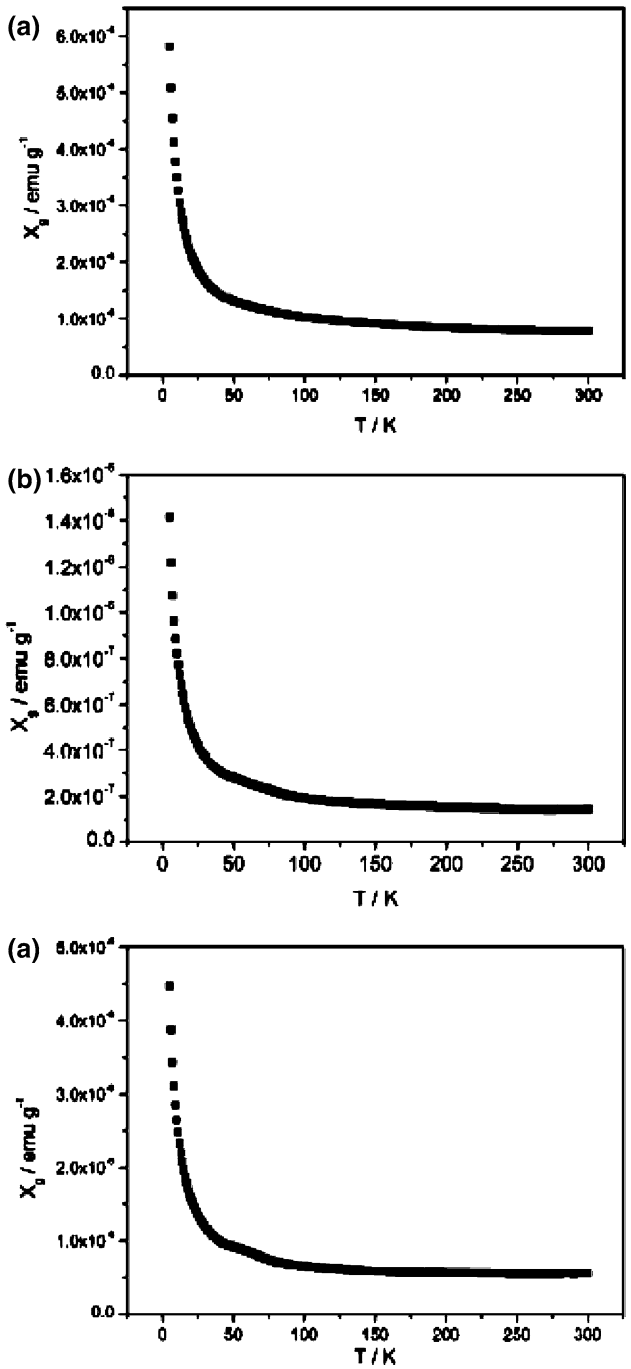

Fig. 7 Plots of mass susceptibility versus temperature for (**a**) $Mo_{1-x}Ta_x(N,O)$, (**b**) $Ta_{1-x}W_x(N,O)$ and (**c**) $Nb_{1-x}Mo_x(N,O)$

for hydrogen transfer reactions. The oxynitrides display weak temperature independent paramagnetism typical of Pauli paramagnets with no evidence of cooperative interactions.

Acknowledgements The authors would like to Ms N Bock and Dr FJ Allison for assistance with SEM and TEM measurements. DHG and WY would like to thank the Royal Society for awarding WY a Sino-British Fellowship and for funding this work. DHG would also like to thank the EPSRC for the award of an Advanced Research Fellowship.

References

1. Disalvo FJ (1990) Science 247:649
2. Kerlau M, Merdrignac-Conanec O, Reichel P, Barsan N, Weimar U (2006) Sens Actuators B Chem 115:4
3. Florea M, Silvy RP, Grange P (2003) Appl Catal A Gen 255:289
4. Jansen M, Letschert HP (2000) Nature 404:980
5. Fabregas RP, Marin JI, Cascales C, Puche RS (2007) J Solid State Chem 180:92
6. Gajbhiye NS, Ningthoujam RS (2006) Mater Res Bull 41:1612
7. Schottenfeld JA, Benesi AJ, Stephens PW, Chen G, Eklund PC, Mallouk TE (2005) J Solid State Chem 178:2313
8. Gregory DH (1999) J Chem Soc Dalton Trans 259
9. Delasarte S, Florea M, Mauge F, Grange P (2006) Catal Today 116:216
10. See for example: Yashima M, Maeda K, Teramura K, Takata T, Domem K, Chem Phys Lett 416 (2005) 225; Centeno MA, Paulis M, Montes M, Odriozola JA, Appl Catal B 61 (2005) 177; Florae M, Silvy RP, Grange P, Appl Catal A 286 (2005) 1
11. Maeda K, Teramura K, Saito N, Inoue Y, Domen K (2006) J Catal 243:303
12. Mientus R, Grotschel R, Ellmer K (2005) Surf Coat Technol 200:341
13. Iriyama Y, Kako T, Yada C, Abe T, Ogumi Z (2005) J Power Sour 146:745
14. Marco De Lucas MC, Fabriguette F, Linsavanh M, Imhoff L, Heintz O, Josse-Courty C, Mesnier MT, Potin V, Bourgeois S, Sacilotti M (2004) J Cryst Growth 261:324
15. Wong CK, Wong H, Chan M, Kok CW, Chan HP (2006) Microelectron Reliab 46:2056
16. Jung WS (2006) Mater Lett 60:2954
17. Delasarte S, Grange P (2004) Appl Catal A: 259:269
18. Nowak I, Ziolek M (2006) Catal Today 118:410
19. Li Y, Gao L (2003) Mater Lett 57:1062
20. Matylistskaya VA, Bock W, Thoma K, Kolbesen BO (2005) Appl Surf Sci 252:205
21. de Graaf D, Hintzen HT, de With G, Ramanujachary KV, lanci C, Lofland SE (2004) Solid State Commun 131:693
22. Katsumata T, Takaki S, Inaguma Y, Shan YJ (2004) Solid State Commun 132:583
23. Casadei F, Pileggi R, Valle R, Matthews A, Surf Coat Technol 201 (2006) 1200; Himri AE, Sapiña F, Ibañez R, Beltrán A, J Mater Chem 11 (2001) 2311
24. Boultif A, Louer D (1991) J Appl Cryst 24:987
25. Nolze G, Kraus W (1998) Powder Diffract 13:256
26. Ruth K, Kieffer R, Burch R (1998) J Catal 175:16
27. Botella P, López Nieto JM, Solsona B, Mifsud A, Márquez F (2002) J Catal 209:445
28. Afanasiev P, Fischer L, Beauchesne F, Danot M, Gaborit V, Breysse M, Catal Lett 64 (2000) 59; Trunov VK, Kovba LM, Sirotkina EI, Dokl Akad Nauk SSSR 153 (1963) 1085
29. See for example: Herle PS, Hegde MS, Vasathacharya NY, Philip S, Rama Rao MV, Sripathi T (1997) J Solid State Chem 134:120
30. Volpe L, Oyama ST, Boudart M (1983) Stud Surf Sci Catal 16:147
31. Oyama ST, Kapoor R, Oyama HT, Hoffmann DJ, Matijevic E (1993) J Mater Res 8:1450
32. Jackson SK, Layland RC, Zur Loye H-C (1999) J Alloys Compd 291:94
33. Clarke SJ, DiSalvo FJ (1997) J Solid State Chem 132:3